Journal of Materials Chemistry A

Accepted Manuscript

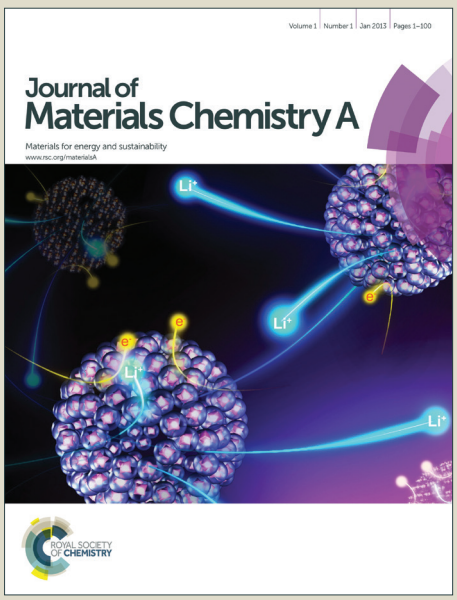

ROYAL SOCIETY OF CHEMISTRY

www.rsc.org/materialsA

Crumpled reduced graphene oxide by flame-induced reduction of graphite oxide for supercapacitive energy storage†

Yan-Zhen Liu[a], Cheng-Meng Chen[a,], Yong-Feng Li[b,]*, Xiao-Ming Li[a], Qing-Qiang Kong[a], and Mao-Zhang Wang[a]*

Abstract: A novel flame-induced synthesis approach was developed to prepare crumpled reduced graphene oxide (rGO) from graphite oxide (GO) powder with the assist of flammable polar solvents such as methanol, ethanol and acetone under ordinary conditions. The as-prepared methanol-rGO, ethanol-rGO and acetone-rGO exhibit the high surface area of 421, 500 and 384 $m^2 g^{-1}$, respectively. The method is highly attractive for the mass production of graphene due to its simplicity, high efficiency, energy saving and cost-effective. The thermal exfoliation and reduction of GO powder, as well as the morphology and surface chemistry of resulting rGO, was related to the volatility, infiltration and combustion heat of the solvents. The electrochemical properties of the rGO samples were further evaluated in 6 M KOH aqueous electrolyte. In a three-electrode setup, the corresponding specific capacitance of methanol-rGO, ethanol-rGO and acetone-rGO were calculated to be 260, 221 and 200 F g^{-1} at a current density of 0.1 A g^{-1}, respectively. Moreover, the flame-reduced methanol-rGO exhibited the maximum energy density of 68.85 Wh kg^{-1} as tested in a two-electrode system. The excellent supercapacitive performance of the methanol-rGO and ethanol-rGO materials is attributable to the combination of high surface area, residual oxygen containing groups and wrinkled morphologies.

Keywords: Graphene; Reduction; Combustion; Flammable solvent; Supercapacitor

[a]Key Laboratory of Carbon Materials, Institute of Coal Chemistry, Chinese Academy of Sciences, Taiyuan, Shanxi, 030001, China. E-mail: ccm@sxicc.ac.cn

[b]Yangquan Coal and Chemical Industry Group Co., Ltd, Taiyuan, Shanxi, 030001, China. E-mail: gocsjn@163.com

†Electronic supplementary information (ESI) available: Nine figures and one table showing further details of the samples. See DOI:

1. Introduction

Supercapacitors have attracted tremendous attention as ideal energy storage devices for load cranes, forklifts, memory back-up systems and electric vehicles to meet the growing demands of long cycle life, excellent cycling stability, as well as high power density, short load time, and low maintenance cost.[1-3] Numerous materials have been explored to fabricate supercapacitor electrodes, including carbonaceous materials, conductive polymers, and transition metal oxides.[4-6] Based on charge storage mechanisms stemming from various active materials, supercapacitors are generally divided into two types: electrochemical double-layer capacitors (EDLCs) and pseudocapacitors.[7,8] While in EDLCs, energy storage takes place by ion adsorption between electrode-electrolyte interface, pseudocapacitor store energy by fast and reversible Faradic reactions at or near the solid electrode surface. However, such "pseudocapacitors" often result in compromises of rate capability and reversibility because they rely on faradic redox reactions and the active materials are typically too insulating to support fast electron transport required by high rates. Comparing with pseudocapacitors, longer life time, lower cost and higher power density can be attained for EDLCs. Hence, carbonaceous materials such as activated carbons, carbon fabrics, carbon nanotubes, and graphene are widely used as electrode materials for EDLCs.[2,9]

Graphene, a one-atom-thick sheet of carbon atoms arranged in a honey-comb lattice, is regarded as a potential candidate for EDLCs due to its intriguing characteristics, such as high theoretical surface area of 2630 $m^2 g^{-1}$ and intrinsic in-plane electron mobility as well as high mechanical strength and chemical stability.[10-14] Currently, various graphene-based materials are intensively investigated as supercapacitive electrode materials, such as reduced graphene oxide (rGO) materials by chemical or thermal reduction of graphite oxide (GO) in a large scale at low cost[15-18]. For instance, Stoller et al. explored a symmetric supercapacitor based on chemically reduced GO to give a specific capacitance of 135 F g^{-1} in KOH and 99 F g^{-1} in organic electrolytes, respectively.[19] Chen et al. reduced GO by $NaBH_4$, and then

produced thin film of chemically reduced GO by vacuum filtration, which exhibited a specific capacitance of 135 Fg^{-1} in 2 mol L^{-1} KCl electrolyte.[20] Vivekch et al. fabricated a capacitor from thermal exfoliated (1050 ^{o}C) GO electrodes to obtain capacitance of 117 F g^{-1} in 1 mol L^{-1} H_2SO_4 and 75 F g^{-1} in $PYR_{14}TFSI$.[21] However, the facts that the reducing agents such as hydrazine or $NaBH_4$ are toxic and dangerously unstable while the high temperature exfoliation process is energy-consuming, make it highly desirable to develop other green and efficient approaches of GO reduction in the perspective of industrial applications.

Flame synthesis, a self-propagating high-temperature synthesis technique, has been used successfully to grow diverse materials including low- dimensional carbon structures such as carbon nanotubes, fullerenes, sheet-like carbon particles and amorphous carbon thin films.[22-25] Li et al. reported a dual flame synthesis method which was applied to generate graphene/graphite films directly on the surface of nickel foils in ambient conditions.[23] Recently, Sun et al. prepared rGO paper by a rapid and clean flame-induced reduction of GO paper using a common lighter, which contains butane liquid.[26] However, to the best of our knowledge, the thermal exfoliation and reduction of GO powder into rGO by combustion in a flammable solvent has not been reported yet.

Herein, we present a rapid, simple, scalable and low-cost method to prepare wrinkled rGO by a flame-induced reduction of GO powder immersed in a flammable polar solvent such as ethanol, methanol and acetone under ordinary conditions. The microstructure and surface chemistry of combustion derived ethanol-rGO, methanol-rGO and acetone-rGO were systemically characterized by X-ray diffraction (XRD), X-ray photoelectron spectroscopy (XPS), Fourier transformation infrared spectroscopy (FTIR), scanning electron microscopy (SEM) and transmission electron microscopy (TEM) techniques. The electrochemical supercapacitive properties of the crumpled rGO were further evaluated in a KOH aqueous electrolyte, so as to provide an insightful material chemistry towards designing of advanced graphene based electrode materials for energy storage applications.

2. Experimental

2.1 Preparation of graphite oxide (GO) powder

GO was synthesized from natural graphite powder by a modified Hummers' method as described elsewhere.[10] The graphite powder was oxidized through a strong oxidation using $KMnO_4$, $NaNO_3$, 98% H_2SO_4. The as-prepared GO hydrogel was vacuum dried at 50 ^oC and then grinded into fine GO powder (*ca.* 300 mesh).

2.2. Preparation of rGO

In a typical experiment, 3 g of GO powder was mixed well with excess ethanol (methanol/acetone) to obtain swelled GO powder. Then the swelled GO powder was burned by ignition using a matchstick under ordinary conditions, while a cylindric metal net was set above the flame to collect rGO powder. Black rGO powder was obtained within several seconds. The as-prepared products were denoted as ethanol-rGO, methanol-rGO and acetone-rGO according to the ethanol, methanol and acetone solvents, respectively.

2.3. Materials characterizations

The crystallographic structures of the materials were determined by a powder X-ray diffraction system (TTR-III) equipped with Cu-Ka radiation (λ= 0.15406 nm). Surface chemistry information was collected by X-ray photoelectron spectroscopy (Thermo ESCALAB 250). Fourier transform infrared spectra were run on a Bruker Model IFS 66 v/s spectrophotometer. Raman spectra were performed on a SPEX-1403 Raman spectrometer with 514.4 nm excitation source from an Ar^+ laser. The specific surface areas were measured using the Brumauer-Emmett-Teller (BET) method based on the nitrogen adsorption- desorption isotherms measured at 77 K on a Micromeritics TriStar II 3020 sorption analyzer. The topographic morphology of the materials was characterized by atomic force microscopy (AFM) (Tip mode, Agilent Technologies, Agilent 5500 AFM/SPM System). Scanning electron microscopy and transmission electron microscopy observations are conducted using Nova NanoSEM 430, FEI and JEOL2010F, respectively.

2.4. Electrochemical measurements

The electrochemical properties of the as-prepared ethanol-rGO, methanol-rGO and acetone-rGO powders were measured in a 6.0 M aqueous KOH electrolyte. The

three-electrode experimental setup was employed for the measurements. A nickel foam coated with a certain amount of electrode materials pressed under 10 MPa served as the working electrode, a platinum foil electrode and a standard Hg/HgO electrode served as the counter and reference electrodes, respectively. To prepare the electrode materials, a certain amount of rGO materials was mixed with 5% polytetrafluoroethylene (PTFE) binder, and then an amount of ethanol was added dropwise. The mixture was ground with a mortar and pestle until a homogeneous, cohesive blend was obtained, followed by a 12 h drying at 100 ^{o}C in a vacuum oven to remove the ethanol and moisture. These electrodes were soaked in a 6 M KOH solution for 12 h. The performance of the material was analyzed on a CHI760D Electrochemical Working Station using cyclic voltammetry (CV), galvanostatic charge/discharge (GC), and electrochemical impedance spectroscopy (EIS). The EIS was fitted with the Zview software. The average specific capacitance was estimated from the discharge slope according to the following equation:[27] $C=(I\times\Delta t)/(\Delta V\times m)$, where C is the specific capacitance, I is the current loading (A), Δt is the discharge time (s), ΔV is the potential change during discharge process, and m is the mass of the active material in the electrode (g). To further evaluate the supercapacitor performance, the electrodes were configured in a two-electrode test cell consisting of two current collectors, two electrodes, and a nickel foam supported in a test fixture consisting of two stainless steel plates, the detail procedures and calculated equation of specific capacitance were shown in Supporting information. In addition, it is confirmed that the contribution of nickel foam support ($C_{Ni} \approx 0.067$ F g^{-1}) to the specific capacitance of the sample during electrochemical test is negligible (Fig. S8†).

3. Results and discussion

The synthesis is schematically illustrated in Scheme 1. Firstly, the GO powder prepared by modified Hummers' method from natural graphite was impregnated by a flammable polar solvent such as ethanol, methanol and acetone. The wet GO powder was ignited using an ordinary matchstick under ambient conditions. Immediately, the fluffy black powder was floated over the flame and collected by the metal wire mesh. Interestingly, this reduction process was very rapid and the GO powder was partially

reduced, as indicated by the color change from deep brown to black. The possible mechanism based on the flame-induced reduction of GO assisted by flammable polar solvents was investigated. The precursor GO, as synthesized by liquid phase oxidation and intercalation of natural graphite, exhibit an expanded interlayer space of up to 0.6-0.8 nm and highly hydrophilic surface. The material will be easily solvated or swelled when exposed to vapor or immersed in a polar liquid solvents. Additionally, a flame is the visible, gaseous part of a fire, which is caused by a highly exothermic reaction taking place in a thin zone. If hot enough, the gases may become ionized to produce plasma. Sufficient energy in the flame will excite the electrons in some of the transient reaction intermediates (eg. Carbon free radicals), resulting in the emission of visible light as these substances release their excess energy. Take ethanol as an example, the GO powder can be swelled after mixing with ethanol. The combustion of ethanol provides not only high temperature but also carbon source. Thus, the GO powder can be reduced within several seconds without any metal catalysts. Compared with the ethanol-chemical vapor deposition (CVD) technique,[22,25] this approach is very rapid, simple, and cost-effective for high quality graphene products, as the resulting materials with high purity for avoiding the possible contamination by metal catalyst.

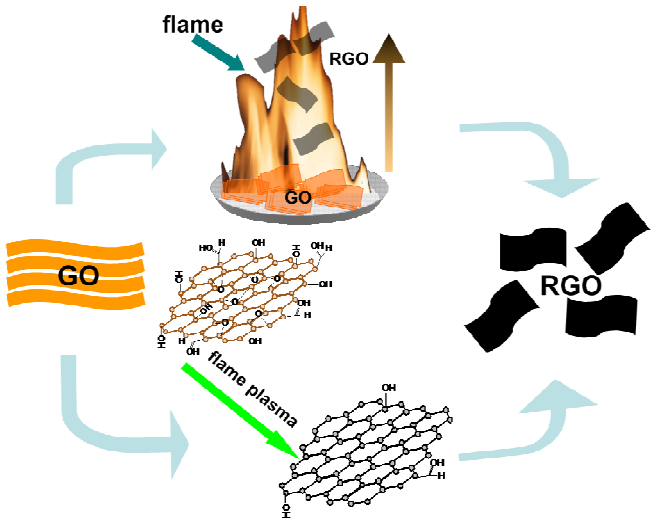

Scheme. 1 Schematic illustration of preparation of rGO by a flame-induced reduction.

The pore structure of the samples was quantitatively analyzed by the nitrogen adsorption and desorption isotherms, as shown in Fig. 1. According to the IUPAC classification,[28,29] the nitrogen adsorption isotherms of all samples are characterized as type IV with hysteresis loops, implying the presence of a large number of mesopores due to the formation of crumpled and folded few-layered graphene sheets (Fig. 1a). The BET surface areas of ethanol-rGO, methanol-rGO, and acetone-rGO are determined to be 500, 387 and 426 $m^2 g^{-1}$, respectively. These values are significantly lower than the theoretical surface area of 2630 $m^2 g^{-1}$, which indicates an average overlap and stacking of *ca.* 5-6 layers of graphene sheets in the obtained materials[30,31]. This is also corroborated by the AFM (Fig. S1†) and HRTEM images (Fig. S2†). The maximum surface area obtained for the ethanol-rGO is consistent with the adequate exfoliation during the reduction due to the sufficient swell of GO powder in ethanol that its volatility is weaker than that of methanol and acetone. As shown in Fig. 1b, the pore-size distributions from the adsorption branch of the isotherms using the Barrett-Joyner-Halenda (BJH) method reveal the broad distribution of mesopores from 2 to 100 nm for all samples. The difference in pore structures of different rGO samples will affect their final capacitor performances.

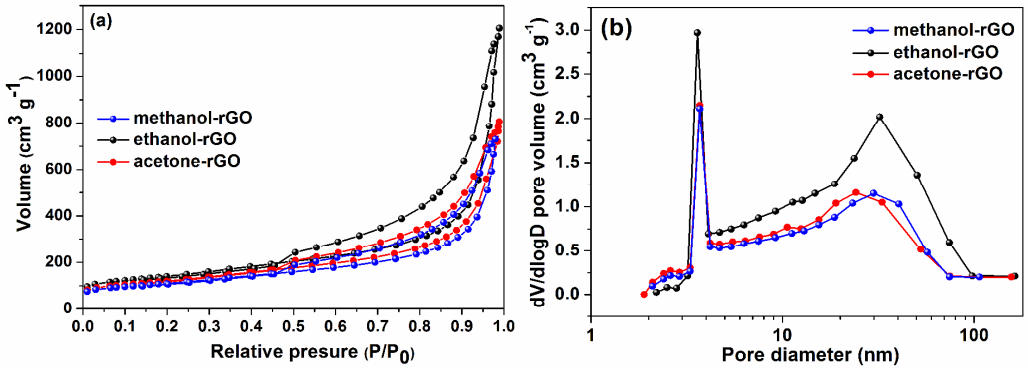

Fig. 1 (a) N_2 adsorption-desorption isotherms and (b) pore size distributions of ethanol-rGO, methanol-rGO and acetone-rGO.

XPS was used to reveal the nature of carbon and oxygen bonds in the pristine GO powder and the resulting rGO samples obtained by the flame-induced process. As shown in Fig. 2a, the atomic ratios of carbon to oxygen for ethanol-rGO, methanol-rGO and acetone-rGO samples are 6.92±0.03, 6.38±0.16 and 7.91±0.12

respectively, which are much higher than that of GO (1.69), indicating a substantial elimination of oxygen containing groups in the flame-induced reduction.[32-34] In order to further identify the functional groups of the as-prepared rGO samples, the XPS C1s peaks were analyzed using a peak fitting procedure that employs a combination of Gaussian and Lorentzian functions (Fig. S3†). The structural changes from GO powder to graphene sheets during the reduction process are also reflected in FTIR spectra (Fig. S4†) and XRD patterns. There are still a small amount of oxygen present in the rGO samples, specially for methanol-rGO. From the high resolution O1s spectra shown in Fig. 2b, two peaks centered at 530-532 eV and 533 eV can be assigned to C=O type oxygen groups and the C-O-C type oxygen or C-OH oxygen groups, respectively.[12,33] Despite the dramatic removal of the dominant C-O peaks in comparison with that of GO, all rGO samples exhibit relatively more C-O-C and/or C-OH type oxygen than C=O type oxygen, suggesting the repair of the π network in graphene lattice, which is in good agreement with the previous reports.[26,34,35] The peak of O1s spectra of methanol-rGO is stronger than that of ethanol-rGO and acetone-rGO, implying a lower reduction efficiency which is attributable to the inadequate swelling of GO in methanol. In the combustion process, the thermal induced interlayer exfoliation will enlarge the surface area, while the restoration of sp^2 hybridized carbon by thermal reduction will improve the electrical conductivity of the resulting material. This dual effect is desirable to enhance the supercapacitive performance of the resulting material. Additionally, it has been widely demonstrated that surface functional groups containing oxygen, nitrogen, or phosphorus can considerably enhance the total capacitance through additional faradaic reactions, as well as improving the wettability of porous carbon with electrolytes.[36] Thus, it can be deduced that the higher oxygen composition in methanol-rGO is also beneficial for supercapacitors through reversible pseudo-faradic reactions.

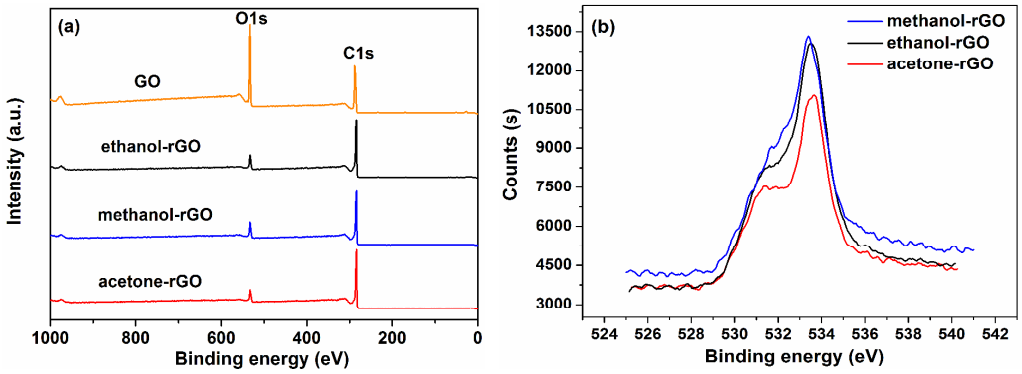

Fig. 2 (a)XPS general spectra and (b) O1s spectra of ethanol-rGO, methanol-rGO and acetone-rGO.

The powder XRD patterns of the precursor GO and resulted rGO samples were depicted in Fig. 3a. A typical broad (001) peak near 10.75° with an enlarged interlayer spacing of 0.822 nm was observed for the GO powder, as a result of the incorporation of water and oxygen functional groups during the oxidation process.[29,32] After combustion induced thermal exfoliation, the typical peak of parent GO around 10.75° was disappeared in rGO, indicating the well exfoliation and deoxygenation of GO. Besides, very weak peaks at around 25° (002) in all rGO samples, with a corresponding d_{002} space (0.35 nm) larger than the pristine graphite (0.34 nm), is attributable to the irregular stacking of wrinkled graphene sheets.[16] It is noteworthy that a weak (001) peak of methanol-rGO located at 10.75° is still identified, implying the inadequate interlayer exfoliation and reduction, which is associate with the XPS and FTIR results. Moreover, the $\Delta_c H^{\ominus}$ (enthalpy of combustion) values of methanol, ethanol, and acetone are 715.0 kJ/mol, 1371 kJ/mol and 1785.7 kJ/mol, respectively. From these data, it can be seen that the $\Delta_c H^{\ominus}$ value of methanol is the smallest, which may lead to the incomplete combustion and lower reduction degree of GO powder.

Furthermore, the reduction of GO by the flame-induced method is evidenced by Raman spectroscopy (Fig. 3b). All samples display two prominent peaks corresponding to the well-documented D and G bands, respectively. The D band is associated with the defects, while the G band corresponds to the vibration of sp^2-bonded atoms in a two-dimensional hexagonal lattice related to the order of the sample.[37,38] The peak for GO (1597 cm^{-1}) at the G band was up-shifted compared with

that of pristine graphite (1583 cm^{-1}).[17] This difference was attributed to the presence of isolated double bonds in the GO sample, which resonate at frequencies higher than that of the G band of the graphite.[12] The G band of the three rGO samples occurred at 1586 cm^{-1}, which attributes to the recovery of the hexagonal network of carbon atoms with defects. In addition, the integrated intensity ratio of the D and G band (I_D/I_G) of GO is about 0.92. Interestingly, the I_D/I_G ratios of acetone-rGO, methanol-rGO and ethanol-rGO are around 0.866, 0.856 and 0.836, respectively. The I_D/I_G ratios of the as-prepared rGO samples are lower than that of most chemical reduction reports, such as $NaBH_4$ (1),[39] hydrazine hydrate (1.63) [40] or thermal reduction at 1000 ^oC (1.17),[17] indicating good defect repairs and more effective than the other reduction process. From the previous works, researchers synthesize graphene on metal support by a CVD method using ethanol and methanol as carbon sources.[41] The mechanism of repairing defects of rGO during the reduction may called "self-healing". The flammable polar solvents such as acetone, methanol and ethanol can act not only as burning materials but also as carbon sources. Compared with the chemical structures of acetone, methanol and ethanol, free radicals such as CH·, CH_3·, CH_3-CH_2· originated fromethanol in burning are prone to deposit on the graphene sheets. Thus, the aliphatic alcohols such as methanol or ethanol are better used as liquid fuels for preparation of graphene materials.

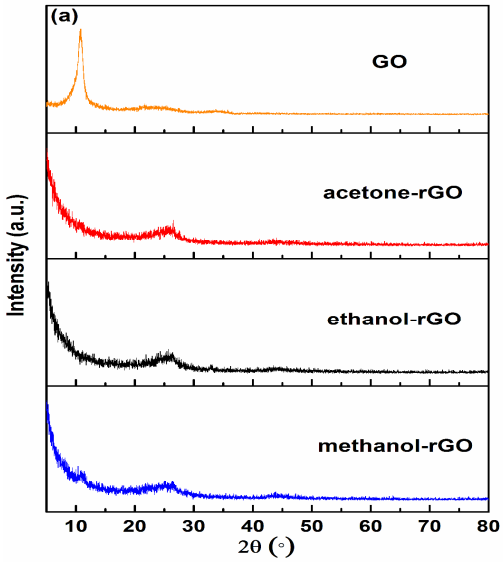

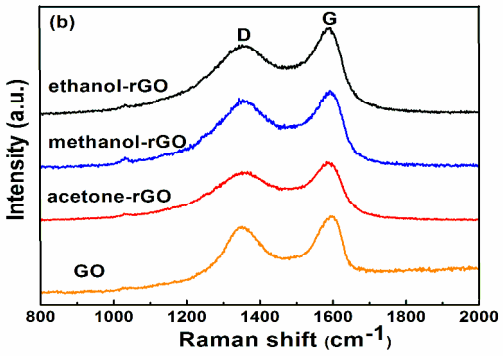

Fig. 3 (a) XRD patterns and (b) Raman spectra of GO, ethanol-rGO, methanol-rGO and acetone-rGO.

The morphology of the as-synthesized rGO samples was characterized by FESEM and TEM (Fig. 4). From the FESEM images (Fig. 4a-c), all rGO samples exhibit a typical curved/wrinkled appearance, as a result of the decomposition of the oxygen functional groups that leads to graphene-like sheets with a disordered stacking. Notably, for graphene, contact between different regions of graphene could lower the total energy through Vander Waals cohesion and stabilize the crumpled phase.[30] Compared with methanol-rGO and acetone-rGO, the ethanol-rGO displayed a higher porous structure attributed to the folded and crumpled few-layered graphene sheets, which is also confirmed by the BET results. Furthermore, the TEM images of all rGO samples also show multilayer graphene sheets with wrinkled structures. Recent literatures demonstrated that the mesopores and wrinkles on the surface of graphene sheets may shorten the ion diffusion lengths in supercapacitors, leading to electrodes with improved performance.[30,31,42]

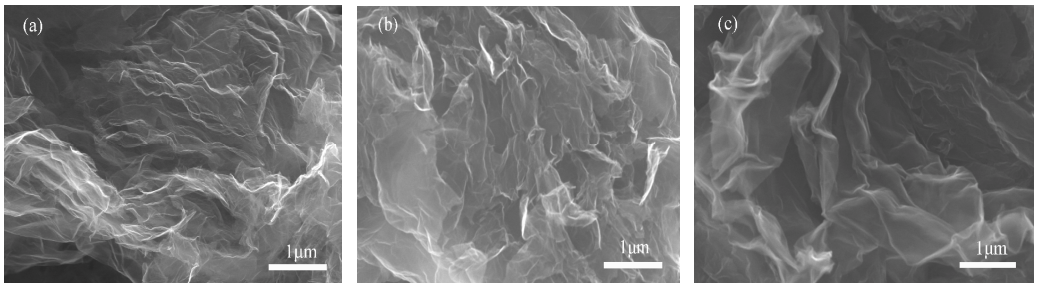

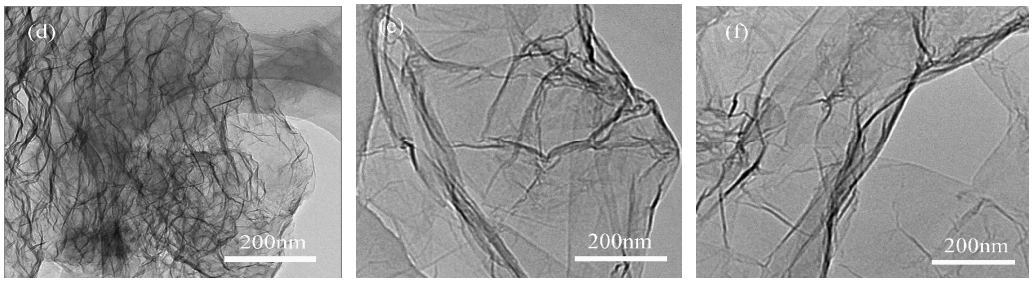

Fig. 4 SEM and TEM images of (a,d) ethanol-rGO, (b,e) acetone-rGO and (c,f) methanol-rGO, respectively.

The electrochemical properties of the as-prepared three rGO samples were studied by performing CV using a three-electrode system, as shown in Fig. 5a. The CV curves are nearly rectangular in shape at a scan rate of 5 mV s^{-1} in a 6 M KOH aqueous solution, indicating good charge propagation within the electrodes.[29,42] As seen from the methanol-rGO curve, a broad peak at around -0.7 V is observed, which could be attributed to the residual oxygen groups. Among the three rGO samples, the residual oxygen-containing groups of methanol-rGO are the highest, which is in accordance to the XRD and XPS results. The oxygen-containing groups in rGO samples, especially epoxy and alkoxy result in fast redox processes in methanol-rGO, leading to additional pseudocapacitive contribution along with the EDLC behavior giving rise to larger specific capacitance values.[26,36] Compared with acetone-rGO, the CV curves of the methanol-rGO and ethanol-rGO are close to rectangular at various scan rates (Fig. S5†) and even at a high scan rate of 100 mV/s, indicating an excellent capacitance performance and low contact resistance in the capacitors.

Fig. 5b shows GC curves of the as-prepared three rGO samples at a constant current density of 1 A g^{-1}, displaying a nearly linear response for the excellent capacitive behavior. From Fig. S6†, all of the charge-discharge curves at different current densities were good symmetry and fairly linear, again demonstrating the capacitive behavior. Methanol-rGO exhibits a larger current response in CV curves as well as a longer charge-discharge time in GC curves, implying a larger capacitance than ethanol-rGO and acetone-rGO. The specific capacitance was calculated from the galvanostatic discharge branch (Fig. 5c). Under a specific current density of 0.1 A g^{-1}, the specific capacitances of methanol-rGO, ethanol-rGO and acetone-rGO, were

calculated to be 260, 224.5 and 212.6 F g^{-1}, respectively. The specific capacitance values obtained for the as-prepared rGO samples in present study based supercapacitors are better than those reported by Wang et al. [14] and Luo et al. [30] The value for methanol-rGO is comparable to that reported by Zhao et al.(260.5 F g^{-1} at 0.4 A g^{-1}) [43] for rGO synthesized by thermal reduction of GO.

More detailed comparison of electrode performance of graphene-based materials in the literatures is shown in Table S1†. As shown in Fig. 5c, it is shown that the specific capacitance decreases with the increase of current density, which is in consistent with other reports.[26,29,30] Moreover, the methanol-rGO and ethanol-rGO samples delivered a specific capacitance of 98.9 and 95.7 F g^{-1} at a high operation rate of 20 A g^{-1}, whereas the acetone-rGO yielded only 12.9 F g^{-1}. These results showed that methanol-rGO and ethanol-rGO exhibited better rate performance than acetone-rGO. In order to confirm the electrochemical supercapacitive performance in real applications, the as-prepared materials were further estimated in a two-electrode cell with a potential ranging from 0 to 0.9 V. As shown in Fig. S7†, all the materials exhibit typical capacitive behavior with quasi-rectangular shape in CV curves and symmetry triangle pattern in GC curve. The specific capacitances of methanol-rGO, ethanol-rGO and acetone-rGO were determined to be 170, 147.9, 144.8 F/g at a current density of 0.1 A/g, respectively. The energy densities based on two electrode cell-type supercapacitor were calculated to be 68.85, 59.9, 58.65 Wh/kg at a corresponding power density of 185.1, 191.5, 192.4 W/kg, respectively.

In order to investigate the transport characteristics within the rGO based supercapacitor electrodes, the electrochemical impendence spectroscopy (EIS) measurement is carried out at open circuit potential over a frequency range of 10 kHz to 10 mHz. As shown in Fig. 5d, Nyquist plots of EIS data for methanol-rGO, ethanol-rGO and acetone-rGO exhibited a semicircle over the high frequency range, followed by a linear part in the low frequency region. The depressed semicircle in the high-frequency region is modeled by a parallel combination of an interfacial charge transfer resistance and the double-layer capacitance.[2] The inset was the typical equivalent circuit of different elements from the EIS analysis. The equivalent series

resistance (ESR) of methanol-rGO, ethanol-rGO and acetone-rGO electrodes obtained from the intersection of the Nyquist plot at the *x*-axis is 1.93 Ω, 0.42 Ω and 1.92 Ω, respectively. Compared to the ESR of 3.7 [2] and 4.638 Ω [44] from other graphene based supercapacitors reported previously, the values in present study is significantly smaller, which indicate less internal energy loss with better power performance. Moreover, as evaluated by a four point probe method, all the rGO samples exhibit quite high electrical conductivity in a range from 150 to 500 S/m, which is of great importance for electrode materials (Fig. S9†).

The Nyquist plot at high frequency (the straight line) is the resistance resulting from the frequency dependence of ion diffusion/transport.[28]The straight lines of methanol-rGO and ethanol-rGO are steeper than that of acetone-rGO, suggesting faster ion diffusion and closer behavior to ideal capacitors.[42] All of the reasons indicated that the rGO samples, especially methanol-rGO and ethanol-rGO are potential advanced electrode materials for supercapacitors.

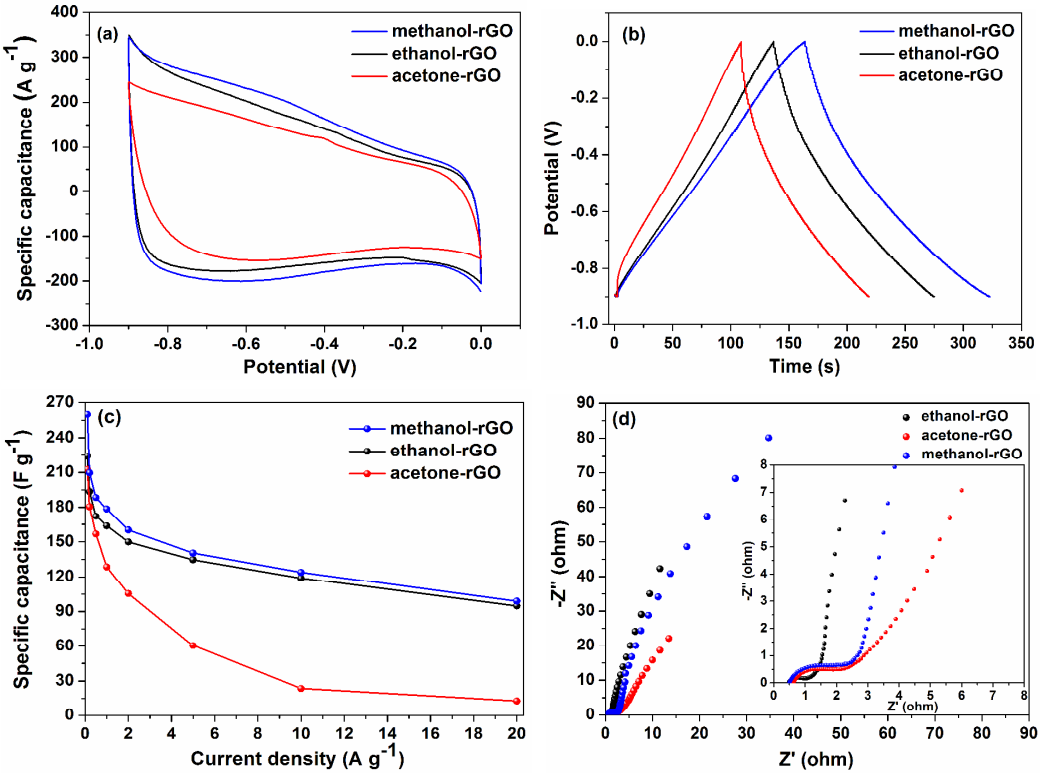

Fig. 5 Electrochemical results based on a three-electrode setup: (a) CV curves of methanol-rGO, ethanol-rGO and acetone-rGO samples at a scan rate of 5 mV s^{-1}; (b) GC curves of the as-prepared rGO samples at a constant current density of 1 A g^{-1}; (c) Specific capacitance of samples at

different current densities; (d) EIS of samples; the inset shows the enlarged EIS at the low frequency region.

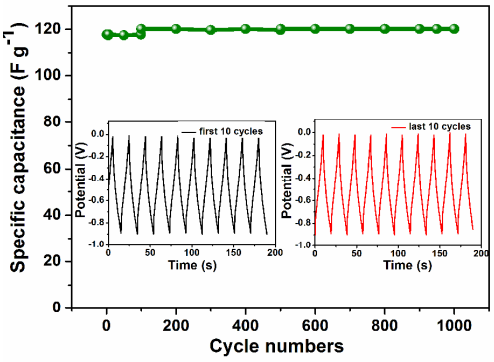

Fig. 6 Charge/discharge cycling test based on a three electrode setup for ethanol-rGO at a current density of 10 A g^{-1}; inset shows the GC curves of the first and last 10 cycles.

The advantages of composite electrode methanol-rGO and ethanol-rGO based electrode over the acetone-rGO for supercapacitors were clearly demonstrated. Considering the safety in burning process and similar performance in electrochemical properties, the ethanol is proposed to be more suitable as burning solvent for graphene preparation. Additionally, the cycling stability of the ethanol-rGO electrode in KOH aqueous solution between -0.9 to 0 V was investigated at a constant current density of 10 A g^{-1}. As shown in Fig. 6, the specific capacitive retention was 100% after 150 cycles. Interestingly, compared with many previous reports on supercapacitors based on rGO samples,[26,27,29,36] the ethanol-rGO obtained here by the flame-induced reduction method yields an improvement of 5% after 1000 cycles in terms of specific capacitance. The last 10 cycles remained almost the same shape but a bit longer of charge-discharge time with the first 10 cycles (insets in Fig. 6). The enhanced capacity may be attributed to the improvement of ion accessibility in crumpled graphene sheets during the cycling process which leads to an increased accommodation behavior for charges. These results indicate that the as-prepared rGO samples by the flame-induced reduction with the assist of flammable polar solvents are very promising electrode for supercapacitor materials with high capacity, good cycle performance and high degree of reversibility in the repetitive charge-discharge cycling.

4. Conclusions

We developed a novel flame-induced reduction approach for crumpled rGOs by burning GO powder swelled in a flammable polar solvent such as methanol, ethanol and acetone under ordinary conditions. The solvent not only plays an important role in swelling and heating up the GO powder, but also acts as carbon sources. The new reduction method offers the advantages of simplicity, rapidity, high efficiency, energy saving, low cost and mass production of graphene. The methanol-rGO, ethanol-rGO and acetone-rGO have a high surface area of 421, 500 and 384 m^2 g^{-1}, while the specific capacitances are 260, 221 and 200 F g^{-1} in a three-electrode setup, respectively. The good supercapacitive performances of methanol-rGO and ethanol-rGO in KOH aqueous solutions are benefited from the combination of high surface area, the residual oxygen containing groups and wrinkled morphologies. This scalable and environmental friendly methodology will shed a light for tunable surface chemistry of high quality graphene materials for potential applications in energy storage, catalysis and thermal management.

Acknowledgements

We are grateful for the experimental assistance on GO preparation by Mr. Yuan-Zhi Li, and appreciate the financial support from the Innovative Research Fund of ICC-CAS (2012SCXQT03), National Natural Science Foundation of China (51302281), Natural Science Foundation of Shanxi Province (2013011012-7), Innovative Research Fund of Taiyuan Science and Technology Bureau (2012CXJD0510), and Shanxi Coal Transportation and Sales Group Co. Ltd (2013WT103).

Notes and references

1 T. Y. Kim, G. Jung, S. Yoo, K. S. Suh and R. S. Ruoff, *ACS Nano*, 2013, **7**, 6899.
2 T. Y. Kim, H. W. Lee, M. Stoller, D. R. Dreyer, C. W. Bielawski, R. S. Ruoff and K. S. Suh, *ACS Nano*, 2011, **5**, 436.
3 M. G. Deng and R. Q. Wang, *New Carbon Mater*., 2013, **28**, 261.
4 C.H. Xu, B.H. Xu, Y. Gu, Z.G. Xiong, J. Sun and X.S. Zhao, *Energy Environ. Sci*., 2013, **5**, 1388.
5 Y. F. Li, Z. S. Li and P. K. Shen, *Adv. Mater*., 2013, **25**, 2474.
6 Y. Zhu, S. Murali, M. D. Stoller, K, K. J. Ganesh, W. Cai, P. J. Ferreira, A. Pirkle, R. M.

Wallace, K. A. Cychosz, M. Thommes, D. Su, E. A. Stach and R. S. Ruoff, *Science*, 2011, **332**, 1537.

7 B. Zhang, L. Fan, H. Zhong, Y. Liu and S. Chen, *J. Am. Chem. Soc*., 2013, **135**, 10073.

8 Y. Z. Liu, Y. F. Li, M. Zhong, Y. G. Yang, Y. F. Wen and M. Z. Wang, *J. Mater. Chem*., 2011, **21**, 15449.

9 D. F. Zheng, M. Q. Jia, B. Xu, H. Zhang, G. P. Cao and Y. S. Yang, *New Carbon Mater*., 2013, **28**, 151.

10 C. M. Chen, Q. Zhang, C. H. Huang, X. C. Zhao, B. S. Zhang, Q. Q. Kong, M. Z. Wang, Y. G. Yang, R. Cai and D. S. Su, *Chem. Commun.,* 2012, **48**, 7149.

11 P. Tassin, T. Koschny and C. M. Soukoulis, *Science*, 2013, **341**, 620.

12 I. K. Moon, J. Lee, R. S. Ruoff and H. Lee, *Nature Commun*., 2010, **1**, 1.

13 X. Ding, Z. H. Huang, W. C. Shen and F. Y. Kang, *New Carbon Mater.*, 2013, **28**, 172.

14 Y. Wang, Z. Shi, Y. Huang, Y. Ma, C. Wang, M. Chen and Y. Chen, *J. Phys. Chem. C,* 2009, **113**, 13103.

15 B. G. Rafael, G. B. Herme, L. S. Marcos, A. Mercedes and G. Hermenegildo, *J. Mater. Chem. A,* 2013, **1**, 11728.

16 G. Srinivas, Y. Zhu, R. Piner, N. Skipper, M. Ellerby and R. Ruoff, *Carbon*, 2010, **48**, 630.

17 C. Botas, P. A. Ávarez, C. Blanco, R. Santamaría, M. Grandaa, M. D. Gutièrrez, F. R. Reinoso and R. Menèndez, *Carbon*, 2013, **52**, 476.

18 S. Obata, H. Tanaka and K. Saiki, *Carbon*, 2013, **55**, 126.

19 M. D. Stoller, S. J. Park, Y. W. Zhu, J. H. An and R. S. Ruoff, *Nano Lett*., 2008, **8**, 3498.

20 B. Yuan, T. Zhu, Z. X. Zhang, Z. Y. Jiang and Y. Q. Ma, *J. Mater. Chem*. *A*, 2013, **21**, 3471.

21 K. S. Subrahmanyam, S. R. C. Vivekchand, A. Govindaraj and C .N. R. Rao, *J. Mater. Chem.*, 2008, **18**, 1517.

22 Z. Li, H. Zhu, K. Wang , J. Wei , X. Gui and X. Li , *Carbon*, 2011, **49**, 237.

23 Z. Li, H. Zhu, D. Xie, K. Wang, A. Cao, J. Wei, X. Li, L. Fan and D. Wu, *Chem. Commun*., 2011, **47**, 3520.

24 F. Xu, S. D. Tse, J. F. Al-Sharab and B. H. Kear, *Appl. Phys. Lett*., 2006, **243**, 113.

25 K. P. Rajat, B. Sushmee, N. C. H. Robert, M. B. Veera, C. N. Carmen, N, B. Krassimir and M. Ashok, *Carbon*, 2011, **49**, 3789.

26 D. Sun, X. Yan, J. Lang and Q. Xue, *J. Power Sources*, 2013, **222**, 52.

27 Y. Wang, S. Gai, N. Niu, F. He and P. Yang, *J. Mater. Chem. A*, 2013, **1**, 9083.

28 T. Y. Kim, G. Jung, S.Yoo, K. S. Suh and R. S. Ruoff, *ACS. Nano*., 2013, 7, 6899.

29 Y. Bai, R. B. Rakhi, W. Chen and H. N. Alshareef, *J. Power Sources*, 2013, **233**, 313.

30 J. Luo, H. D. Jang and J. Huan, *ACS Nano*., 2013, **7**, 1464.

31 C. Chang, Z. Song, J. Lin and Z. Xu, *RSC Adv*., 2013, **3**, 2720.

32 D. Kim, S. J. Yang, Y. S. Kim, H. Jung, C. R. Park, *Carbon*, 2012, **50**, 3229.

33 S. J. Yang, T. Kim, H. Jung, C. R. Park, *Carbon*, 2013, **53**, 73.

34 H. Wu, W. Lu, J. J. Shao, C. Zhang, M. B. Wu, B. H. Li and Q. H. Yang, *New Carbon Mater.*, 2013, **28**, 327.

35 T. Zhou, F. Chen, K. Liu, H. Deng, Q. Zhang, J. Feng and Q. Fu, *Nanotechnol.,* 2011, **22**, 1.

36 B. Xu, S. Yue, Z. Sui, X. Zhang, S. Hou, G. Cao and Y. Yang, *Energy Environ. Sci*., 2011, **4**, 2826.

37 H. Wang, J. T. Robinson, X. Li and H. Da, *J. Am. Chem. Soc*., 2009, **131**, 9910.

38 K. Parvez, R. Li, S. R. Punired, Y. Hernandez, F. Hinkel, S. Wang, X. Feng and K. Müllen, *ACS Nano*, 2013, **7**, 3598.

39 H. J. Shin, K. K. Kim, A. Benayad, S. M Yoon, H. K. Park, I. S. Jung, M. H. Jin, H. K. Jeong, J. M. Kim and J. Y. Choi, *Adv. Func. Mater*., 2009, **19**, 1987.

40 J. Yan, Z. J. Fan, T.Wei, W. Z. Qian, M. Zhang and F. Wei, *Carbon*, 2010, **48**, 3825.

41 J. Robin, A. Ashokreddy and T. Pradeepa, *Nanotechnol*., 2011, **22**, 165.

42 S. Zhang, N. Pan, *J. Mater. Chem. A*, 2013, **1**,7957.

43 B. Zhao, P. Liu, Y. Jiang, D. Y. Pan, H. H. Tao, J. S. Song, T. Fang and W. W. Xu, *J. Power Sources*, 2012, **198**, 423.

44 Y. Wang, Z. Shi, Y. Huang, Y. Ma, C. Wang, M. Chen and Y. Chen, *J. Phys. Chem. C,* 2009, **113**, 13103.